Earthquake Engineering, Tenth World Conference © 1992 Balkema, Rotterdam. ISBN 90 5410 060 5

Quantification of soil non-linearity in cyclic loading by the use of Fourier components

Christian Madshus
Norwegian Geotechnical Institute, Oslo, Norway
Yoshiaki Kikuchi
Port and Harbour Research Institute, Yokosuka, Japan

ABSTRACT: A method to quantify the non-linear behaviour of soils subjected to cyclic loading is presented. The method is based on Fourier decomposition of the recorded response time histories from harmonically excited cyclic tests on laboratory samples. It is demonstrated that secant modulus, hysteretic damping and shape of the hysteresis loops may be quantified with sufficient accuracy by six parameters, derived from the three first Fourier components of the measured response.

INTRODUCTION

Due to their non-linear natur, soils respond by hysteretic behaviour when subjected to cyclic loading. The size and shape of the resulting hysteresis loops depend on the soil type and vary throughout a test, depending on stress level and number of load cycles. The objective of the present study was to find a convenient set of parameters that can be used to generally quantify the size and shape of these hysteresis loops. Attention was given to finding a method that requries a minimum of parameters, and to find parameters that are simple to estimate even when the test data contain noise.

1 SOIL MODELLING USING FOURIER COMPONENTS

A soil element subjected to cyclic loading can be considered as a "input/output" system where the response is a function of the excitation and soil properties. The properties of a linear soil are independent of the excitation, and can uniquely be determined by relating response to excitation.

For soils with non-linear behaviour, certain restrictions must be put on the excitation. One useful way to quantify the non-linear properties is to study the response to a pure harmonic excitation:

$$\tau(t) = \tau_o \cdot \cos \omega t \qquad (1)$$

Due to the non-linearity, the response, $\gamma(t)$, will generally not be sinusoidal. However, if the soil properties do not develop as a function of time (t), or if the time dependence can be separated, $\gamma(t)$ will be periodical. It can then be Fourier expanded, according to Eqs 2 and 3:

$$\gamma(t) = a_o + \sum_{n=0}^{\infty} \left[a_n \cdot \sin(n \cdot \omega t) + b_n \cdot \cos(n \cdot \omega t)\right] \qquad (2)$$

$$= a_o + \sum_{n=1}^{\infty} \left[c_n \cdot \cos(n \cdot \omega t - \phi_n)\right]$$

$$\text{Here: } a_n = \frac{1}{T} \int_{-T}^{T} \gamma(t) \cdot \sin(n \cdot \omega t)\, dt$$

$$b_n = \frac{1}{T} \int_{-T}^{T} \gamma(t) \cdot \cos(n \cdot \omega t)\, dt \qquad (3)$$

$$\tan \phi_n = -a_n / b_n$$

The above approach can easily be implemented in cyclic soil testing, where tests on soil specimens are usually run under harmonic load control.

Section 2 will demonstrate that by truncating the Fourier series of $\gamma(t)$ to its three first components, any reasonable non-linear soil behaviour can be modelled with sufficient accuracy for all engineering applications.

2 ANALYTICAL FORMULATION

2.1 *Case of no phase shift between excitation and response*

If the response is not biased, the truncated Fourier expression will read:

$$\gamma(t) = \gamma_o [\cos \omega t + \alpha \cdot \cos 2\omega t + \beta \cdot \cos 3\omega t] \qquad (4)$$

By transforming the cosine expressions for double and tripple angles and eliminating the time (t) by the substitution from Eq. 1, the τ-γ relation for the corresponding soil model will be:

$$\frac{\gamma}{\gamma_o} = \left[\frac{\tau}{\tau_o}\right] + \alpha\left[2\left[\frac{\tau}{\tau_o}\right]^2 - 1\right] + \beta\left[4\left[\frac{\tau}{\tau_o}\right]^3 - 3\left[\frac{\tau}{\tau_o}\right]\right] \quad (5)$$

As seen, the assumption on the response of Eq. 4 leads to a 3rd degree polynomial stress-strain relation, with no discrimination between loading and unloading.

The α-term adds non-symmetry to the stress-strain curve. $\alpha > 0$ gives downward curvature and $\alpha < 0$ has the opposite effect. The β-term adds the "S-shape" to the curve: $\beta > 0$ causes a "stiffening" behaviour, while $\beta < 0$ causes "softening".

The condition that the τ-γ curve should be monotonic puts restrictions on α and β. Figure 1 pictures the set of acceptable values of α and β.

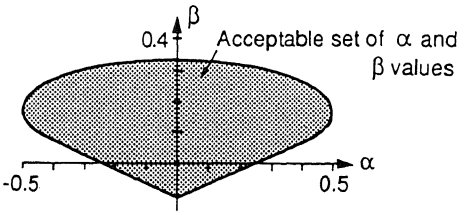

Figure 1. Set of acceptable α and β values.

2.2 *Case of phase shift between excitation and response*

Usually soils respond to cyclic loading by producing open τ-γ hyseresis loops.

In the present approach open loops are obtained by introducing a time shift (Δt), or a phase shift (ϕ), between response and excitation:

$$\gamma(t) = \gamma_o[\cos(\omega t - \phi_1) + \alpha\cdot\cos 2(\omega t - \phi_2) + \beta\cdot\cos 3(\omega t - \phi_3)] \quad (6)$$

The simplest form is obtained for $\alpha = \beta = 0$ and $\phi_1 = \phi \neq 0$, which represents a linear system with viscous or "linear hysteretic" damping.

For the linear hysteretic case, ϕ will be constant. For the viscous case it will increase linearly with frequency.

The corresponding equation of the τ-γ hysteresis loop becomes:

$$\frac{\gamma}{\gamma_o} = \left[\frac{\tau}{\tau_o}\right]\cdot\cos\phi \pm \sqrt{1 - \left[\frac{\tau}{\tau_o}\right]^2}\cdot\sin\phi \quad (7)$$

The negative sign is for the loading part and the positive sign for the unloading part.

The hysteresis loop is a straight line with an ellipse added to it.

The hysteretic damping of the loop is defined as:

$$D = \frac{1}{4\pi}\cdot\frac{W_L}{W_P} \quad (8a)$$

where

$$W_L = \int_o^T \tau(t)\cdot\frac{d\gamma}{dt}dt = \pi\cdot\tau_o\cdot\gamma_o\cdot\sin\phi \quad (8b)$$

i.e. the area enclosed by the loop

$$W_P = \frac{1}{2}\cdot\tau_o\cdot\gamma_o\cdot\cos\phi \quad (8c)$$

i.e the maximum, potential energy.

By substituting for W_L and W_P in Eq. 8a, the damping becomes:

$$D = \frac{1}{2}\tan\phi \quad (9)$$

For a response including all three Fourier components, the strain time history will be expressed by the following if the same phase shift is assumed for all components:

$$\gamma(t) = \gamma_o[\cos(\omega t - \phi) + \alpha\cdot\cos 2(\omega t - \phi) + \beta\cdot\cos 3(\omega t - \phi)] \quad (10)$$

For this case the equation for the corresponding stress-strain loop has the same basic form as Eq. 5, and the coefficients α and β have the same effect on non-symmetry and S-shape of the curve. The effect of the phase shift ϕ, corresponding to a time lag:

$$\Delta t = \phi/\omega \quad (11)$$

is to add width to the loop.

The equation for hysteretic damping for this case yields:

$$D = \frac{1}{4\pi}\cdot\frac{W_L}{W_P} = \frac{1}{2}\cdot\frac{\tan\phi}{1+\beta} \quad (12)$$

For $\alpha \neq 0$ the τ-γ loop is non-symmetrical and $\gamma_{max} \neq -\gamma_{min}$. Defining the secant modulus $\overline{G}_{sec} = \tau_o/\gamma_{max}$ or $-\tau_o/\gamma_{min}$ gives two different values. Here, the following definition was chosen:

$$\bar{G}_{sec} = 2\tau_o/(\gamma_{max} - \gamma_{min}) \qquad (13a)$$

This mean secant modulus will be:

$$\bar{G}_{sec} = \frac{1}{1+\beta} \cdot \frac{\tau_o}{\gamma_o} \qquad (13b)$$

The damping in Eq. 12 is consistent with the $\bar{G}_{sec}$ definition of Eq. 13b.

Equation 10 is somewhat restricted in its ability to describe all variations of hysteresis loops encountered for soils. Required flexibility is obtained by adding some freedom in terms of δ and ε to the phase angle of the 2nd and 3rd harmonic components, leading to the following expression for the strain response:

$$\begin{aligned}\gamma(t) = \gamma_o\{&\cos(\omega t - \phi) + \\ &\alpha\cdot\cos[2(\omega t - \phi) - \delta] + \\ &\beta\cdot\cos[3(\omega t - \phi) - \varepsilon]\}\end{aligned} \qquad (14)$$

with this description of the response, the stress-strain hysteresis loop yields:

$$\begin{aligned}\frac{\gamma}{\gamma_o} = &\cos\phi\cdot\left[\frac{\tau}{\tau_o}\right] + \alpha\cos(2\phi+\delta)\cdot\left[2\left[\frac{\tau}{\tau_o}\right]^2 - 1\right] \\ &+\beta\cdot\cos(3\phi+\varepsilon)\cdot\left[4\left[\frac{\tau}{\tau_o}\right]^3 - 3\left[\frac{\tau}{\tau_o}\right]\right] \\ &\pm\left\{\sin\phi + \alpha\cdot\sin(2\phi+\delta)\cdot\left[\frac{\tau}{\tau_o}\right]\right. \\ &\left.+\beta\cdot\sin(3\phi+\varepsilon)\cdot\left[4\left[\frac{\tau}{\tau_o}\right]^2 - 1\right]\right\}\cdot\sqrt{1-\left[\frac{\tau}{\tau_o}\right]^2}\end{aligned} \qquad (15)$$

In this case, analytical expressions for D and $\bar{G}_{sec}$ have not been derived.

To define criteria that restrict Eq. 15 to describe only geotechnically sound hysteresis loops (monotonicity etc.) and map the limits of α and β, as in Fig. 1 for various values of ϕ, δ and ε, is a complex analytical exercise not performed here.

From an harmonic excitation, Eq. 1, and a response function like Eq. 15, a secant modulus can always be defined. However, since the series of $\gamma(t)$ is truncated, the stress-strain hysteresis curve will always have some "roundness" at its upper and lower ends. The initial (maximum) shear modulus, G_{max} is therefore not defined in the model.

The stress-strain hysteresis loops defined by models, as expressed by the Eqs 5, 7 and 15 all express the strain as a function of the stress, $\gamma(\tau)$. The equations can be inverted to express $\tau(\gamma)$. The $\tau(\gamma)$ formulation will be mathematically close to the formulation of $\gamma(\tau)$.

3 PRACTICAL APPLICATION OF THE MODEL

Soil stress-strain relations, $\gamma(t)$, as those expressed in Eqs 5, 7 and 15 can be considered as soil models, where the behaviour is controlled by the parameters ϕ, α, δ, β and τ_o/γ_o:

$$\gamma\left[\tau\,|\,\frac{\tau_o}{\gamma_o}, \phi, \alpha, \delta, \beta, \varepsilon\right] \qquad (16)$$

In a practical application these parameters will be estimated by processing the recorded strain response time histories from cyclic laboratory tests with harmonic excitation. The parameters have to be made functions of cyclic and static stress or strain level, consolidation stresses, pore pressure, present loading history etc., what ever is relevant for the actual soil type and the actual laboratory test. Methods to estimate the parameters from experimental data are discussed in Section 5.

The usefullness of the model is to quantify non-linearity and development of non-linearity from experimental data.

4 FELXIBILITY OF THE MODEL

To study the flexibility of the model to reproduce different load-deformation hysteresis loop-shapes, numerical simulations were made. Figure 2 presents $\tau(\gamma)$ curves for four different combinations of the parameters ϕ, α, δ, β and ε. The plots are normalized to $\pm$ unity along both the τ and γ axis, i.e. the function $(\tau/\tau_o)(\gamma/\gamma_o)$ from Eq. 15 is plotted.

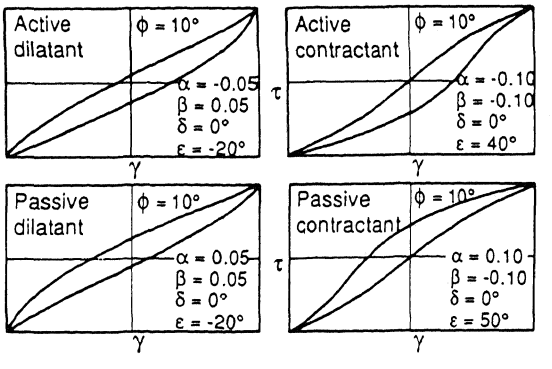

Figure 2. Typical hysteresis loops generated by model.

The figure demonstrates the ability of the model to reproduce an entire family of hysteresis loop shapes usually found in cyclic soil testing.

All loops in the figure were drawn with a phase lag, ϕ, of 10°, corresponding to a hysteretic damping of about 9%. Larger or smaller values of ϕ would have widened or closed the loops and given higher or lower damping.

The parameter, α, controls the up or downwards curvature and thus the non-symmetry of the loops. $\alpha < 0$ gives a shape usually seen in triaxial compression tests and $\alpha > 0$ gives shapes from extension tests.

The parameter, β, controls the S-shape of the loops. $\beta > 0$ gives an increased stiffness towards the max and min points of the loop, usually seen for dilatant soils. $\beta < 0$ gives shapes often seen for contractant soils.

Increasing the absolute value of α or β will exaggerate the characteristic shape of the loops.

The phase angle δ is 0° in all the examples presented. Other values of δ would give minor adjustments to the loop shape without distorting the main characteristics. ε controls the sharpness at the transition between loading and unloading at the max and min points of the loops.

Including more than the three Fourier components used in Eq. 15 will not extend the flexibility of the model, or increase its accuracy in reproducing recorded hysteresis loops beyond what is needed in most egnineering applications.

5 ESTIMATION OF MODEL PARAMETERS FROM LABORATORY TEST RESULTS

The major advantage of the Fourier component soil model is that its parameters can be estimated efficiently and accurately from recorded response time histories from cyclic laboratory soil tests, even if the data are disturbed by noise. The parameter estimation procedure can easily be automated.

If the final goal is to derive parameters for another more commonly used soil model, it will usually be beneficial to derive functional relationships between these parameters and the Fourier component parameters.

The straightforward procedure to estimate the parameters ϕ, α, δ, β, ε and the secant modulus $\overline{G}_{sec}$ is by numerical integration of Eqs 3a and 3b to first detormine a_o, a_1, b_1, a_2, b_2, a_3 and b_3 (i.e. by Direct Fourier Transformation).

From these intermediate results, the parameters can be calculated from:

$$\gamma_o = \sqrt{a_1^2 + b_1^2}\ , \quad \phi = \tan(a_1/b_1)$$

$$\alpha = \sqrt{a_1^2 + b_2^2}\ /\sqrt{a_1^2 + b_1^2}\ , \quad \delta = \tan(a_2/b_2) - 2\phi \qquad (17)$$

$$\beta = \sqrt{a_3^2 + b_3^2}\ /\sqrt{a_1^2 + b_1^2}\ , \quad \varepsilon = \tan(a_3/b_3) - 3\phi$$

By restricting the phase angles δ and ε to the range (90° - 0° and 0° - 90°), α- and β-parameters with negative values are found where the tan-function determines phase angles in the range (90° - 180° and -90° - -180°). When ϕ, α, δ, β, ε, γ_o and τ_o are determined for the data, γ_{max} and γ_{min}, and thus the secant modulus can be calculated from Eq. 15.

For noisy data, there are better procedures to estimate the parameters than the direct Fourier transformation. Procedures based on least square fit or such as the Pisarenko harmonic decomposition algorithms, may give far more stable estimates (Ref. 2).

Digitally filtering the data before parameter determination may improve the results. However, extreme care must be taken to avoid introducing phase errors due to the filtering. Phase shift between stress and strain can easily be avoided by subjecting both signals to exactly the same filter. Relative phase shift, i.e. time lag, or amplitude distortion between the first, 2nd and 3rd harmonic component of the strain signal can be avoided only by using a high quality filter with no phase or amplitude distortion up to three times the excitation frequency.

To avoid frequency leakage and thus inaccurrate estimates of the parameters, it is essential that the integration of Eq. 3 be made over an exact number of complete excitation load cycles. Therefore the integration range can be set only after the excitation frequency f_e is determined. The integration time range is

$$T = n/f_e \qquad (18)$$

where n is an integer number.

For this reason it will usually not be feasible to use Fast Fourier Transform (FFT) algorithms for the parameter estimation. This is because the FFT algorithm puts restrictions (e.g. 2^n) on the number of data points and thus the integration time to be used.

It is also important that the excitation has been purely sinusoidal. However, there are possibilities to correct data from tests with non-sinusoidal excitation, as long as the excitation is regular and well defined.

6 TEST ON SYNTHETIC DATA

The ability of the above model was tested on synthetic data from a multi-surface kinematic hardening soil model.

The model was run in harmonic stress controlled conditions: $\tau(t) = \tau_o \cdot \cos \omega t$.

The resulting $\gamma(t)$ - time history, together with $\tau(t)$ were processed by the procedures described in Section 5 to obtaine the non-linearity parameters, ϕ, α, δ, β and ε. Tests were done at nine shear strian levels ranging from 10^{-4}% to 1.0%.

Figure 3 plots the determined α, β, ϕ_1, $= \phi$, $\phi_2 = (2\phi + \delta)$, and $\phi_3 = (3\phi + \varepsilon)$ versus the cyclic shear strain amplitude, γ_{cy}, in a logarithmic scale. For strains below $3 \cdot 10^{-2}$%, α and $\beta \approx 0$ and the model behaves virtually linearly. At higher strains the β-factor increases significantly while α remains about constant and is very close to 0. To illustrate the extent to which Eq. 15 is able to reproduce the stress-strain hysteresis loops of the kinematic hardening soil model, and to see the deviation due to the truncation of the Fourier series of Eq. 2, to the first three terms, Fig. 4 presents a comparison for stress controlled conditions.

The two curves in the figure present results for $\gamma = 3 \cdot 10^{-1}$%. The figure presents both time histories of stress and strain and strain plotted versus stress in hysteresis loops.

The hysteresis loop shown with solide line represents the behaviour of the kinematic hardening soil model. The dotted loop represents the best fit "Fourier component" model (Eq. 15). The parameters for the "Fourier model" are tabulated to the right in the figure. The values correspond to those presented in Fig. 3.

Minor deviations are visible near the end points of the hysteresis loop. Even for this high non-linearity, the deviation between the two loops never exceeds 3%. The deviations are due to the sharp breaks from loading to unloding in the kinematic hardening model. To represent such sharp breaks frequencies higher than three times the excitation frequency are needed, but real soils never have such sharp breaks.

For all practical purposes, all information on the non-linearity and shape of the hysteresis loops produced by the kinematic hardening soil model is contained in the five parmeters, ϕ, α, δ, β and ε, and the formulation in Eq. 15.

7 TEST ON NOISY LABORATORY DATA

The Fourier component model was tested out on laboratory data from two cyclic triaxial tests on lightly overconsolidated clay.

Each test contained five consecutive "storms", each with six load levels in ascending order. The first one having a cyclic load level of 1/10 of the last one.

The test had a nearly constant average shear stress. At the highest load level of each storm (last level in storm) the shear stress cycled between approximately 0 and 0.8 s_u, where s_u is the undrained shear strength

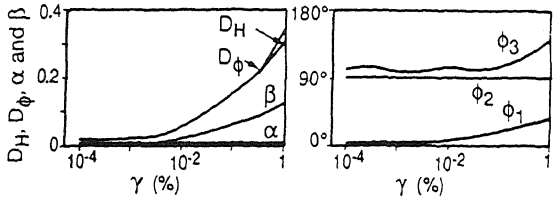

Figure 3. Kinematic hardening model. Damping and parameters.

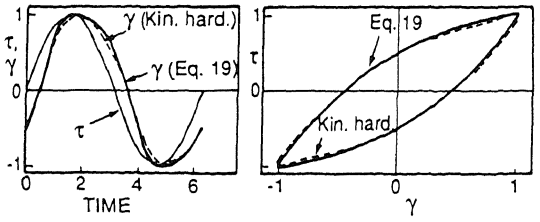

Figure 4. Fit to kinematic hardening model.

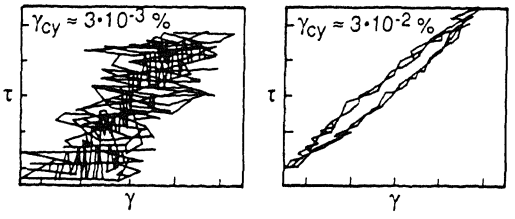

Figure 5. Example on noisy, low strain laboratory data.

from monotonic loading.

Each "storm" contained a total of 240 load cycles. The test covered the cyclic shear strain range from $3 \cdot 10^{-3}$% to 0.75%.

Especially at the lowest strain levels, the signals had a high noise level, as illustrated in Fig. 5.

Data parcels containing five load cycles taken from the beginning and end of each load level from each of the storms, were filtered and processed by the above procedures to determine the "non-linearity" parameters as described in Section 5. For the filtering a "Blanckman-lucky guess filter" with cut off frequency of 6 x excitation frequency was used (Ref. 3).

Figure 6 presents the resulting values of $\phi_1 = \phi$, α, $\phi_2 = (2\phi + \delta)$, β and $\phi_3 = (3\phi + \varepsilon)$ plotted versus cyclic shear strain in a logarithmic scale. The circular symbols are data from the laboratory results. The solide curves are smooth best fit lines through the data.

The damping is mainly controlled by ϕ, and can be approximated by: $D \approx \tan \phi/2$, ref. Eqs 9 and 12.

As seen $D \approx 2\%$ for $\gamma_{cy} \approx 10^{-3}$% and increases to about $\approx 22\%$ for $\gamma \approx 1\%$.

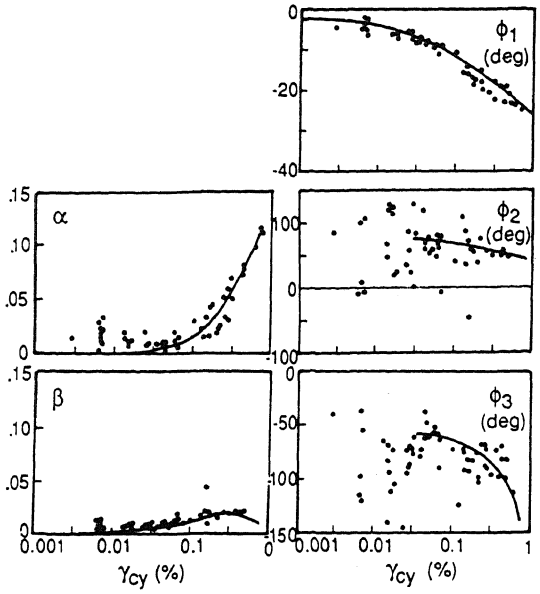

Figure 6. Non-linearity parameters from laboratory data.

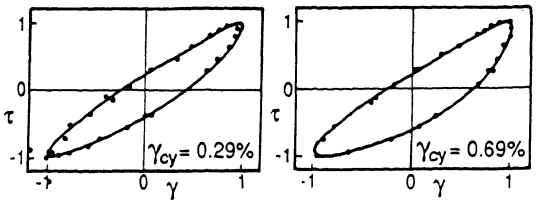

Figure 7. Recorded and regenerated hysteresis loops.

For shear-strains less than $\gamma_{cy} \approx 5 \cdot 10^{-2}\%$, $\alpha \approx \beta \approx 0$ and the soil behaves nearly linearly. For $\gamma_{cy} > 5 \cdot 10^{-2}\%$, the non-symmetry through α dominates. β is small for the entire strain range.

The figure shows scatter in the data, especially at low strains. However, the data seem consistent and conclusive for ϕ, α and β. As expected ϕ_2 and ϕ_3 are undetermined in the range where α and $\beta \approx 0$. Above $\gamma \approx 10^{-2}\%$ also ϕ_2 and ϕ_3 give conclusive values.

A direct comparison is made between the hystresis loops reproduced by the Fourier component soil model, Eq. 15, and directly recorded loops. The comparisons are made at strain levels when the noise in the directly recorded data are not disturbing.

The two hysteresis loops chosen for the comparison have cyclic strain amplitudes of 0.28 and 0.69% respectively. From the smooth, best fit lines in Fig. 6, parameters, ϕ, α, δ, β and ε are picked out at the same strain levels, and synthetic hysteresis loops are constructed from Eq. 15.

Figure 7 plots the results. The loops drawn by solid lines are the synthetic ones from the Fourier Component model. The data points plotted with circular symbols represent smoothed values of the directly recorded hysteresis loops.

The Fourier component soil model gives an excellent average representation of the recorded data points despite the poor signal quality.

CONCLUSIONS

Non-linear, hysteretic soil response to harmonic, cyclic loading, may be represented with sufficient accuracy for any engineering application by three Fourier components. This leads to a hysteretic soil model defined by six parameters which uniquely quantify the secant shear modulus, the hysteretic damping and the shape of the hysteresis loop.

The development of these six parameters throughout a test can easily be determined from recorded stress and strain time histories from cyclic laboratory tests. Stable and reliable estimates of the parameters can be obtained even if the data are disturbed by noise.

It is proposed that the parameters and the method of determination present an efficient and automatic procedure to quantify soil non-linearity in cyclic loading.

ACKNOWLEDGEMENT

The laboratory data referenced are acquired as part of projects for Statoil. The kinematic hardening soil model was developed by SINTEF - Geotechnical Engineering. The authors gratefully acknowledge the contribution from both institutions.

REFERENCES

Kay, S.M. & S.M. Marple, Jr. 1981. Spectrum - analysis - A modern perspective. *Proc. IEEE,* Vol. 69, No. 11: 1380-1419.

Blackman, R.B. & J.W. Tokey 1958. The measurement of power spectra.